Conformations of Self-Avoiding Tethered Chains and Nonradiative Energy Transfer and Migration in Dense and Constrained Systems. A Model for Cores of Polymeric Micelles

David Viduna, Zuzana Limpouchová, and Karel Procházka*

Department of Physical and Macromolecular Chemistry, Faculty of Science, Charles University in Prague, Albertov 2030, 128 40 Prague 2, Czech Republic

Received January 2, 1997; Revised Manuscript Received July 21, 1997[⊗]

ABSTRACT: Monte Carlo simulations of self-avoiding tethered chain conformations in small spherical cavities were performed at relatively high segment densities. Tethered chain systems were studied as models of swollen cores of multimolecular block copolymer micelles in selective solvents. Simulations were performed on a tetrahedral lattice using (i) a mutually independent simultaneous self-avoiding walk of all chains and (ii) a modified equilibration algorithm similar to that proposed by Siepmann and Frenkel [Siepmann, J. I.; Frenkel, D. *Mol. Phys.* **1992**, *75*, 59] for dense polymer melts. Distribution of lengths of tethered end-to-free end vectors, r_{TF}, of individual chains, and their angular orientations, φ, with respect to the radial direction was calculated during computer simulations. Processes of nonradiative energy transfer between end-attached donors and traps and processes of excitation energy migration among identical fluorophores in systems of constrained self-avoiding tethered chains with fluorescently tagged free ends were also studied by computer-based simulations.

Introduction

Since early observations of block copolymer micellization, many micellar properties have been studied by a number of experimental techniques, such as elastic and quasielastic light scattering, ultracentrifugation, viscometry, size-exclusion chromatography, and electron microscopy.[1] In the recent times, steady-state and time-resolved fluorometric techniques with nanosecond or picosecond time resolutions have proved to be powerful and sensitive tools for studying the polymer dynamics in heterogeneous media and in structurally organized polymeric systems[2] and for studying colloidal systems.[3] Fluorometric techniques are particularly valuable in the investigation of properties of micellizing copolymer solutions.[2] Many theoretical studies have also been performed in order to understand the behavior of micellizing polymeric systems.[4,5i] Existing theories are able to predict general properties of copolymer micelles fairly well. However, the detailed knowledge of chain conformations in micellar cores that is needed for correct interpretation of fluorometric measurements with end-tagged insoluble blocks is still limited. Several computer-based studies of the spontaneous association of low-molar-mass detergents and flexible chain molecules (e.g., block oligomers) have been published so far.[5] The published papers represent excellent pieces of computer modeling and yield important information on processes of micelle formation and dissociation; however, due to the complexity of the problem, the chain molecules studied were rather short, and the micellar structure has not been investigated in detail. Valuable information on micellizing polymeric systems has also been obtained indirectly as results of theoretical studies of tethered chains systems. Tethered chains have been studied either by computer-based simulations,[6] or by the scaling approach and the self-consistent field theories.[7] Only little attention has been paid so far to dense systems of tethered chains restricted in small volumes that can be regarded as, e.g., models of micellar cores.[7e,8]

In order to interpret our fluorometric measurements on systems of block copolymer micelles with tagged core-forming blocks in detail,[9] we have recently performed a series of computer-based stochastic simulations[10] on dense systems of chains that are enclosed in a small spherical cavity and are tethered by one end to its surface. In this communication, we present a two-variable distribution function of chain conformations that describes fractions of chains with certain lengths and orientations of end-to-end vectors in constrained systems of tethered chains. Further, we study nonradiative energy transfer from fluorophores to traps in fluorescently tagged systems and processes of excitation energy migration among identical fluorophores and the time-resolved fluorescence anisotropy decays. Simulations are aimed at understanding the conformational behavior of core-forming blocks and the relationship between spatial distributions of end-attached fluorophores and fluorometric data on micellar systems.

Method

The simulation technique used to create equilibrated micellar cores and to evaluate various conformational characteristics of tethered chains was described in detail in our earlier publications.[10] Here we summarize only briefly the fundamentals of the simulation procedure and the most important key steps that are needed to get the equilibrated multichain conformations in a reasonable time.

(1) A simultaneous self-avoiding growth of all N tethered chains is performed in a spherical cavity of a given radius R on a tetrahedral lattice. The tethered ends of chains are located randomly in a narrow surface layer of the thickness Δr_{Surf}; however, the procedure used guarantees a reasonably uniform surface density of tethered ends of chains.

In order to prolong the lth chain in the $(k + 1)$th step, only the unoccupied lattice sites around the kth segment are considered. Various tricks that are described in our papers[10] are used in order to accelerate the creation of systems of N nonintersecting chains with L segments that are used for further equilibration.

* To whom correspondence should be addressed. E-mail: prochaz@vivien.natur.cuni.cz.

[⊗] Abstract published in *Advance ACS Abstracts,* November 1, 1997.

S0024-9297(97)00002-8 CCC: $14.00

The first step is very time-consuming (especially at elevated densities) and must be performed at the maximum possible speed. However this fast simulation algorithm is very biased and does not meet all the requirements of the Monte Carlo simulation. It yields instead nonequilibrium systems for two main reasons: (i) the average segment density increases during the simultaneous growth of all chains; (ii) the biased sampling is used to accelerate the simulations. This sampling considers *a priori* only the unoccupied lattice sites and therefore does not meet correctly the principles of the Monte Carlo method.

(2) The above mentioned bias is corrected in two equilibration steps.

(a) A randomly chosen chain is disregarded, and a new chain grows from a random surface position at the high density. This step is repeated N^2 times to remove the substantial part of the nonphysical effect of the steadily growing density in the first step.

(b) Correction for the biased sampling and the final equilibration is performed using the Rosenbluth weights[11] as follows: A random chain l is disregarded, and a new self-avoiding chain is grown from a random surface place. The Rosenbluth weights, $w_1^{(k)}$, are calculated in each step, k, of the growth of the lth chain. The total weights, $W_1 = \prod_k w_1^{(k)}$, of the new and the old lth chain are evaluated, and a modified Metropolis type acceptance rule[12] (based on the W_{new}/W_{old} ratio) is applied to accept or to refuse the new chain. New chains are grown independently from each other, and they are therefore statistically uncorrelated. Our algorithm is similar to that proposed by Siepmann and Frenkel[13] for dense polymer melts. The last step is repeated until N^2 new chains are accepted, and the system composed of the N last accepted chains is considered as one equilibrated micellar core.

The calculated distribution functions are based on 5×10^4 equilibrated cores which represents a total number of 10^{11} of all generated segment positions—i.e., positions that were either accepted, or refused (since they did not lead to nonintersecting systems, or were not accepted on the basis of the Metropolis-like acceptance rule). At high densities of 0.6−0.7, the fraction of accepted segment positions is only ca. 10^{-3}. Calculations were performed on a workstation INDY XL-8 R4600SC/133 MHz, Silicon Graphics, Inc. Programs were written in FORTRAN 77. The longest calculations took up to 1 month of the CPU.

All attempts to employ equilibration algorithm based on local moves of chain segments as an independent test for the ergodic behavior of simulated systems failed since it was impossible to equilibrate dense systems in acceptable times (the fraction of accomplishable moves at high densities was below 10^{-4}). It was the main reason why the Siepmann and Frenkel algorithm was used because it works well at high densities.

Calculated Functions. The function providing global conformational characterization of tethered chains in the constrained system is the distribution function $P_{TF}^{(r)}(r_{TF}, \varphi)$. This function gives the probability density that a length of the tethered end-to-free end vector is r_{TF} and that this vector simultaneously forms an angle φ with the radial direction defined from the tethered end of the chain to the center of the sphere. The function $P_{TF}^{(r)}(r_{TF}, \varphi)$ is constructed as a histogram during the simulation procedure as follows: (i) a system of narrow concentric layers of the thickness $\Delta r = 1.25l$ with the common center in the tethered end of a chain, and (ii) a system of narrow cones with the apex in the tethered end (apex angle φ increases by increments of $\Delta\varphi = 5°$) are created in the cavity (see the two-dimensional schematics in Figure 1). If the free end of the chain is located in the intersection of spherical and conical volumes defined by $(r_{TF}, r_{TF} + \Delta r\rangle$ and $(\varphi, \varphi + \Delta\varphi\rangle$, i.e., in the sectorial ring of the volume $\Delta V = 2\pi r_{TF} \sin\varphi\, r_{TF}\Delta\varphi\Delta r$ (two cross-sections of this ring are shown in Figure 1), one count is added to the corresponding channel. The above described spherical and conical systems are created around all tethered ends in all equilibrated micelles, and the obtained numbers of chains, $N_{TF}^{(tot)}(r_{TF}, \varphi)$, are normalized *per* unite volume and one chain, i.e., they are divided (i) by average numbers of the lattice sites in corresponding sectorial rings, $\Delta N_{(lat)}(r_{TF}, \varphi)$, (ii) by the number of chains *per* one micelle, N, and (iii) by the number of equilibrated micelles, M, to get the probability density function. Distribution functions $\rho_{TF}(r_{TF})$ and $\psi_{TF}^{(r)}(\varphi)$ that we have presented in our earlier communications[10] may be obtained by averaging $P_{TF}^{(r)}(r_{TF}, \varphi)$ either over the distances r_{TF}, or over the angles φ, taking into account the dependence of the normalization volume element dV on r_{TF} and φ.

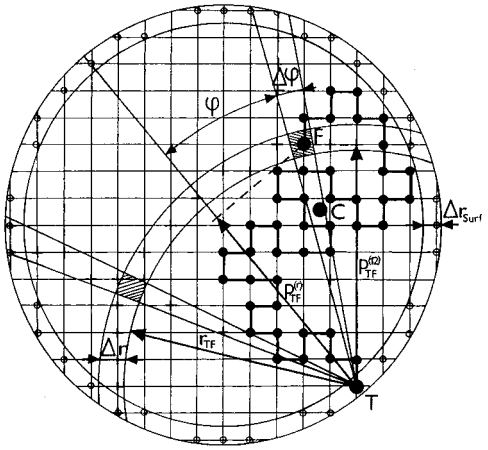

Figure 1. Two-dimensional schematics explaining the evaluation and the normalization principle of the distribution function $P_{TF}^{(r)}(r_{TF}, \varphi)$.

The second class of functions important for interpretation of fluorometric measurements are the normalized distribution functions of mutual distances of free chain ends, $n_{FF}(r_{FF})$ and $\rho_{FF}(r_{FF})$. The function $n_{FF}(r_{FF})$ is also constructed as a histogram during the simulation. The whole range of distances, $2R$, is divided into $1.25l$-wide channels. All $N(N-1)/2$ pair distances are scanned, and counts are added into corresponding channels. The numbers of counts in individual channels are then divided by number of simulated cores and number of free-end pairs in the individual cores. The function $\rho_{FF}(r_{FF})$ is obtained by further normalization of $n_{FF}(r_{FF})$ as follows: values of $n_{FF}(r_{FF})$ in individual channels are divided by numbers of pairs of lattice sites with distances corresponding to appropriate channels. This function was presented for various combinations of N and L in our earlier papers.[10]

Results and Discussion

Since properties of dense systems are controlled mainly by the exclusion volume effect of segments, we have studied the simplified systems (without attractive and long distance repulsive forces) first. The simplified description of interactions affects the calculated func-

tions at high densities only a little. However, the main reason for this choice is the following: We have found in our earlier studies that constrained systems of tethered chains behave differently from other types of polymers.[10] It is therefore necessary to study a relatively simple and well-defined reference system first. The system of self-avoiding chains with purely geometric excluded volume effect of segments captures all important properties of real flexible chains and is a good reference system for our studies. Similar simple systems, e.g., hard sphere fluids,[14] are used as reference systems in other fields of physical chemistry. Careful studies of the behavior of an appropriate reference system allows for differentiation between general properties of self-avoiding tethered chains and specific effects caused by interactions. Studies on that subject are in progress, and results will be published soon.

Recently, we have studied conformational behavior of tethered chains in small spherical volumes in a broad range of average segment densities, ranging from very low values up to the high density $\langle g_S \rangle = 0.75$ that corresponds to compact micellar cores in fairly selective solvents. Systems with the lowest densities (below ca. 0.25) do not correspond to micellar cores; nevertheless, these simulations provide information, e.g., on the behavior of end-adsorbed flexible chains in small spherical pores. Data that we have published earlier[10] show that the simulated density of segments is constant within the cavity and conformational characteristics of tethered chains remain the same at the semiquantitative level for densities higher than ca. 0.25, irrespectively of the combination of N and L. In other words, the basic shape of various distribution functions does not change. Absolute values of these functions do, they depend both on N and L and allow to study important trends in the conformational behavior of core-forming blocks. Therefore we do believe that the tethered chain systems model reasonably well swollen micellar cores (which may be prepared, e.g., by solubilizing small organic molecules into nonpolar cores of polyelectrolyte micelles in aqueous media[9]) and that our simulations yield correct semiquantitative prediction of the conformational behavior of core-forming blocks despite the fact that our simulations do not allow for thermodynamic optimization of the system.

Figure 2 shows the function $P_{TF}^{(r)}(r_{TF}, \varphi)$ that describes the conformational behavior of tethered chains. The function presented is the distribution of lengths of tethered end-to-free end vectors and their angular orientations with respect to the radial direction for systems composed of (a) $N = 35$ tethered chains, each containing $L = 160$ segments, (b) $N = 52$ and $L = 108$, and (c) $N = 70$ and $L = 80$. The average segment density in the core of the radius $R = 15l$ is always $\langle g_S \rangle = 0.6$. The function $P_{TF}^{(r)}(r_{TF}, \varphi)$ is presented in the landscape format as a hypersurface above the plane defined by r_{TF} and φ variables. Curves $P_{TF}^{(r)}(r_{TF}, \varphi =$ constant) for low values of φ resemble the end-to-end distribution functions of nonconstrained self-avoiding chains at infinite dilution. Despite the fact that the concentration of core-forming blocks is fairly high, the constrained chains studied demonstrate an effective nonintersecting behavior (they decrease to zero for small r_{TF}). The studied dense systems of constrained tethered chains do not behave as ideal systems of intersecting chains (recognized theories predict that dense systems of nonconstrained self-avoiding chains mimic the behavior of ideal chains without the excluded volume effect[15]). The shape of the distribution function is also depicted in the form of contours corresponding to constant values, $P_{TF}^{(r)}(r_{TF}, \varphi) =$ constant. The map of contours is shifted below the base plane to gain a comprehensible figure.

In a system composed of 70 relatively short chains with $L = 80$ segments, individual chains are distributed quite uniformly in all allowed directions. Orientations of relatively stretched and fairly oblique chains are excluded by the impermeable surface. The distribution function for the system with a high number of short chains depends more on r_{TF} than that for a system with a low number of long chains. The latter function is flatter and broader which means that the long chains spread more easily in the core, which is not surprising.

Simulation of Nonradiative Energy Transfer. Nonradiative energy transfer (NRET) has been often used to study distributions of pendant fluorophores in various polymeric systems.[2] NRET occurs through induction of a dipole oscillations in an unexcited acceptor or trap by the excited donor. Its rate, $w(r_{ij})$, depends very strongly on the distance, r_{ij}, between the donor i and the trap j and it may be expressed by the Förster formula[16]

$$w(r_{ij}) = (1/\tau_0)(R_0^F/r_{ij})^6 \qquad (1)$$

where τ_0 is the fluorescence lifetime of the donor in the absence of traps and R_0^F is the Förster radius. It is the distance for which the depletion rates of the excited state by energy transfer and by fluorescence are equal. The Förster radius, R_0^F, depends on the mutual orientation of two fluorophores and is given by the formula[17] $R_0^F = \kappa^{1/3} R_0$, where R_0 is the critical radius, which depends on the spectral overlap in the absorption and emission spectra of the pair of fluorophores, and κ is the orientation factor. In the system of randomly oriented fixed fluorophores, the average value of κ^2 is $\langle \kappa^2 \rangle = 0.476$.[17]

We assume a mixed assembly of tagged and nontagged chains as a model for interpretation of fluorometric data on micellar systems with a low fraction of fluorophores attached at the ends of core-forming blocks (a low fraction of tags is often used in experimental studies in order to facilitate the analysis of the data). Micellar systems studied consist of N_o nontagged copolymer chains, N_D chains that are tagged by the donor at the end of the insoluble block, and N_T chains tagged by the trap. The tagged and the nontagged chains are virtually identical except that they either contain or do not contain covalently bound fluorophores at their free ends. In micellar systems with nonpolar insoluble blocks (such as polystyrene) tagged by nonpolar fluorophores (such as naphthyl or anthryl derivatives), interactions between tag−tag, segment−segment, and tag−segment pairs do not significantly differ, and it may be in the first approximation considered that distributions of free ends in labeled and nonlabeled systems are mutually similar and are controlled mainly by the exclusion volume effect of segments. In this communication, we assume that mutual angular orientations of pendant fluorophores are random and do not depend on chain conformations. Since all pendant fluorophores are trapped in fairly rigid micellar cores, both the rotational and translational diffusion of fluorophores in dense polymeric systems proceed on an incomparably longer time scale than the fluorescence decays. Positions and orientations of fluorophores are

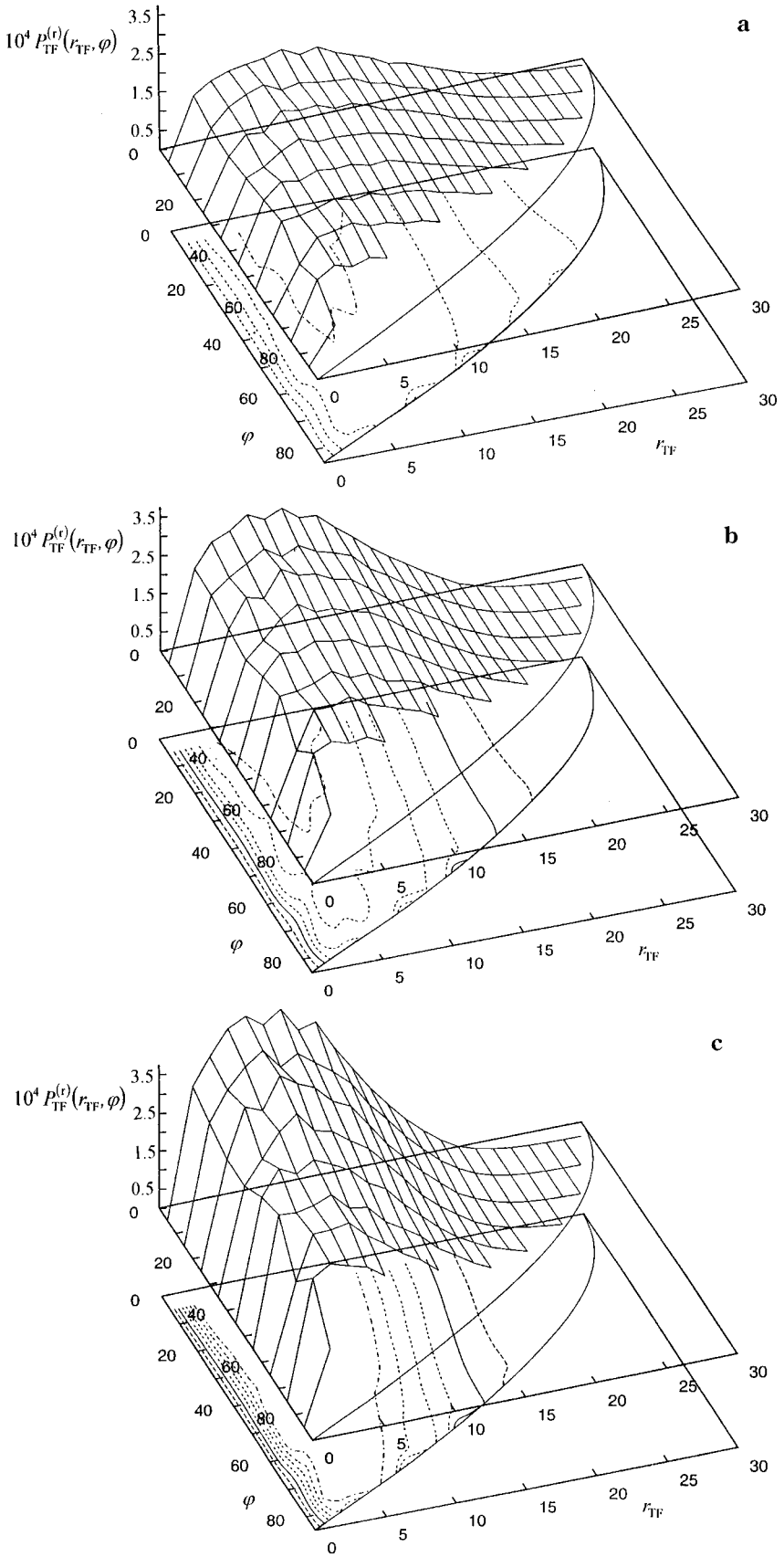

Figure 2. Function $P_{TF}^{(r)}(r_{TF}, \varphi)$ describing distribution of lengths and orientations of end-to-end vectors of self-avoiding tethered chains in the core of the radius $R = 15l$ for the following dense systems of N tethered chains, each containing L segments: $N/L = 35/160$ (a), 52/108 (b), and 70/80 (c). The solid curve in the base-plane shows the geomerical constraint imposed by the impermeable spherical surface of the core. Distribution functions are shown both in the three-dimensional landscape format and as a two-dimensional map of contours $P_{TF}^{(r)}(r_{TF}, \varphi) = \text{constant}$.

therefore fixed and do not change while the excited state of the donor is depleted. We have performed simulations for systems with one energy donor and several traps since it corresponds to experimental conditions in

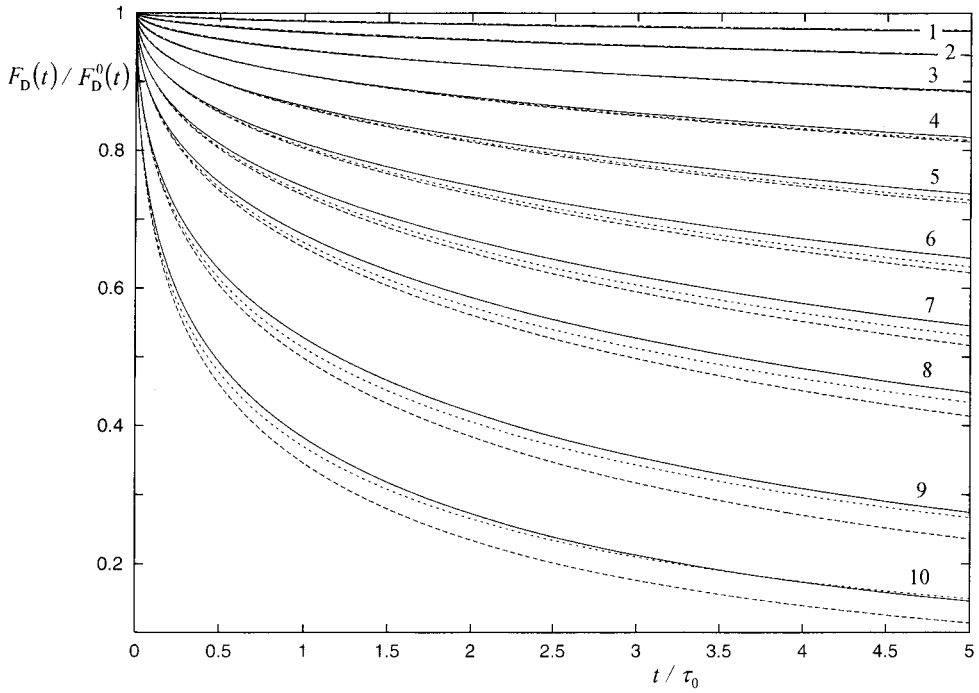

Figure 3. Normalized time-resolved donor fluorescence decays for systems composed of $N = 52$ chains containing $L = 108$ segments for the following values of the Förster radius: $R_0^F = 1.5l$ (1), $2.0l$ (2), $2.5l$ (3), $3.0l$ (4), $3.5l$ (5), $4.0l$ (6), $4.5l$ (7), $5.0l$ (8), $6.0l$ (9), and $7.0l$ (10). Full curves represent systems with nine randomly distributed fluorophores (one donor and eight traps) in each core (RD-FNT), long-dashed curves systems with nine free end-attached fluorophores (one donor and eight traps) in each core (SD-FNT), and short-dashed curves systems with the Poisson distribution of free end-attached fluorophores among micelles (one donor and eight traps on average) (SD-PDT). The radius of the spherical core is $R = 15l$.

fluorometric measurements when only a low fraction of fluorophores are excited (less than one per micelle). We are studying (i) systems with fixed numbers of traps in all micelles (FNT) and (ii) systems with the Poisson distribution of traps among micelles (PDT).

The normalized donor fluorescence intensity decay, $F_D(t)$, in a macroscopic system of multimolecular block copolymer micelles that contain on average one donor, $N_D = 1$, and N_T traps *per* micellar core of the radius R, is the ensemble average of decays from a large number of cores. This decay is described by[18]

$$F_D(t) = F_D^0(t)[\int_0^{2R} \exp[-w(r)t]P(r)\,dr]^{N_T} \qquad (2)$$

where $F_D^0(t)$ is the normalized donor fluorescence decay in the absence of traps, $w(r)$ is the rate of NRET, and function $P(r)$ is the distribution function of distances of donor-trap pairs.

In systems with the end-tagged tethered chains, the distribution function $P(r)$ may be expressed by the simulated distribution $n_{FF}(r_{FF})$, which was defined in the section Calculated Functions and whose values were presented in our earlier papers,[10] and eq 2 may be rewritten into the following form:

$$F_D(t) = F_D^0(t)[\int_0^{2R} \exp[-w(r_{FF})t]n_{FF}(r_{FF})\,dr_{FF}]^{N_T} \qquad (3)$$

In the case that individual micelles in the ensemble do not contain the same number of traps (which is very common in mixed experimental systems), distribution of traps among micellar cores may be expressed by appropriate normalized distribution function, $f(N_T)$. We use the Poisson function since it describes the distribution of fluorophores in real micellar systems fairly well.[19] Experimental fluorescence decay from the donor, $F_D^{ef}(t)$, represents in this case the weighted average over the ensemble of micelles

$$F_D^{ef}(t) = F_D^0(t) \sum_{N_T=0}^{N} f(N_T) [\int_0^{2R} \exp[-w(r_{FF})t]n_{FF}(r_{FF})\,dr_{FF}]^{N_T} \qquad (4)$$

where N_T and N are the number of traps and the number of all chains *per* one micelle, respectively. On the basis of our simulated data, one could calculate the desired average for any distribution of traps.

The relative time-resolved donor fluorescence decays, $F_R(t) = F_D(t)/F_D^0(t)$, were calculated for several micellar systems differing in the number of fluorophores in micellar cores. Effect of energy transfer increases with increasing number of traps in the system which is a trivial consequence of eq 3. For this reason, curves for only one system with one donor and eight traps are shown in Figure 3. Full curves represent decays for systems with random spatial distribution of traps and fixed number of traps in all micelles (RD-FNT), e.g., for systems with traps that have been solubilized in micellar cores. RD is evaluated on the basis of fractions of pairs of lattice sites with corresponding separations in the spherical cavity. The long-dashed curves represent decays for systems with a fixed number of end-attached traps, $N_T = 8$, in all micelles (SD-FNT), for several increasing values of the Förster radius, R_0^F. These decays were evaluated using the simulated spatial distributions of fluorophores (SD). The short-dashed curves describe simulated systems with the Poisson distribution of end-attached traps among micelles (SD-PDT), with $\langle N_T \rangle = 8$.

NRET is weak in systems with low R_0^F values, and the relative decay curves for both RD and SD systems decrease very slowly with time. Mutually corresponding decays are almost indistinguishable despite the fact that

the fraction of pairs with small separations is higher in RD than in SD systems. Decay curves, $F_D(t)/F_D^0(t)$, for random and simulated distributions are mutually well discernible for medium and high R_0^F values. For $R_0^F \geq 0.3R$, the fluorescence decay is slightly faster in SD systems since the total fraction of donor−trap pairs with intermediate separations (i.e., the fraction of pairs that significantly contribute to NRET under given conditions) is higher in SD than in RD systems (see Figure 8 in ref. 9c). It is evident that the energy transfer processes are slightly slower in systems with the Poisson distribution of traps than in systems with a fixed number of traps *per* micelle. The fluorescence behavior of systems with a broad distribution of traps among micelles is a fairly complex one. Equation 4 is nonlinear both in N_T and r_{FF} and cannot be analyzed in a straightforward manner. However, it is shown in Appendix 1 that the observed excitation energy transfer is generally less pronounced in systems with the Poisson distribution of traps (PDT) than in systems with the fixed number of traps (FNT).

Theoretical calculations indicate that differences in fluorescence decays between FNT and PDT systems are generally small. Individual systems (FNT and PDT) are discernible either in the case of higher numbers of traps *per* micelle, N_T, or larger Förster radii, R_0^F. In these cases, systems with random (RD) and simulated (SD) spatial distributions of traps (both for FNT and PDT systems) are also discernible. Nevertheless, curves for different systems studied are generally similar to each other and it is almost impossible to discriminate experimentally between individual systems. This fact is important for interpretation of unusual experimental time-resolved fluorescence decays from some micellar systems. The shape of a particular experimental fluorescence decay curve, which differs considerably from that obtained by simulations, suggests that the spatial distribution of fluorophores in the experimental system is significantly influenced by other factors and differs considerably from the unperturbed reference system (e.g., strong specific interactions between certain functional groups in the polymer chain may lead to the formation of fluorophore clusters and perturb the originally studied system).

The aforementioned simulations show the most important predicted features and trends in fluorometric data based on NRET in micellar cores. In order to establish the direct physical relevance of our model calculations for interpretation of real experimental results, calculations for systems modeling large realistic micellar cores are desirable.

Micelles that we have been studying experimentally,[9] contain typically $(1-2) \times 10^2$ of associated block copolymer chains, each containing ca. $(2-4) \times 10^2$ of core-forming repeating units. Routine computer simulations for such large systems are practically infeasible. Nevertheless, we have recently performed few simulations approaching the size of realistic micellar cores,[20] e.g., $N = 100$ and $L = 160$ at the density of occupied lattice sites, $\langle g_S \rangle = 0.6$. It took more than 2 months of CPU time on an INDY workstation. The study was aimed to find if simulations on smaller systems (that are, e.g., studied in this paper) yield reliable semiquantitative data on realistic polymeric micelles. The answer was positive.

In this work, we use the $\rho_{RR}(r_{RR})$ function obtained in the above mentioned studies.[20] The function $\rho_{RR}(r_{RR})$ is the simulated pair distribution of distances between

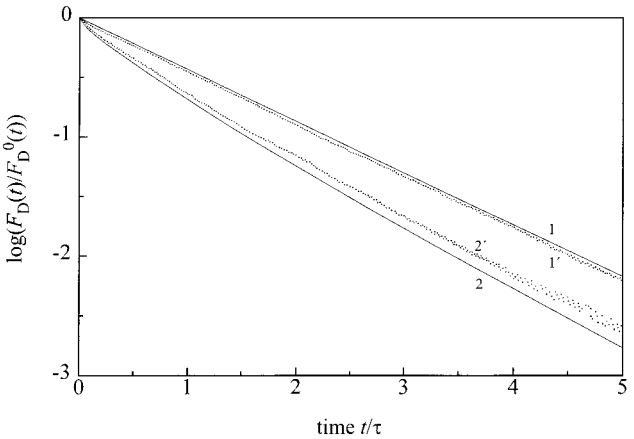

Figure 4. Comparison of NRET experiment[9a] with simulation. In the experiment, micelles formed by carbazole- and anthracene-tagged polystyrene-*block*-(hydrogenated isoprene) samples in a heptane (95 vol %)−1,4-dioxane mixture were studied. The tags (less than one tag *per* chain) were attached randomly at the core-forming polystyrene block. The average number of associated chains *per* micelle was 117, and the average number of anthracene-tagged chains was ca. 70. The radius R_C of the core was ca. 13 nm, and the Förster radius was ca. 2.9 nm. Density of the core was 0.65 g·cm^{-3}. For further detail see ref 9a. The simulated system consisted of 100 chains with a length of 160 segments; 60 chains were tagged at random by traps. The cavity radius was 21.5*l*, and the Förster radius was 4.3*l*. The segment density was 0.6. Curves 1 and 1′ represent simulated and experimental donor decays without NRET, respectively, and curves 2 and 2′ represent corresponding decays affected by NRET for the conditions described above.

fluorophores that are randomly attached at the core-forming blocks. Using this function we are comparing simulated and experimental data for micelles with a random attachment of tags at the core-forming blocks. Figure 4 shows the measured and calculated donor (carbazole) fluorescence decays from micelles formed by carbazole-tagged copolymer (curve 1′) and from mixed micelles that contain ca. 70 acceptors (anthracene) and ca. 30 carbazole units, (curve 2′). However, due to the low excitation intensity, only a very low fraction of donors (less than one donor *per* micelle) is excited. The copolymers studied experimentally were carbazole- and anthracene-tagged polystyrene-*block*-(hydrogenated isoprene) samples with a random attachment of tags at the polystyrene block. The fluorescence decays were measured in a heptane (95 vol %)−1,4-dioxane mixture,[9a] where micellar cores formed by polystyrene are partially swollen (radius of the core R_C is ca. 13 nm and their density is ca. 0.65 g·cm^{-3}). Since the density of the glassy polystyrene is ca. 1.0 g·cm^{-3}, a reliable comparison requires simulations for the density of occupied lattice sites ca. 0.65. Simulations have been done for a very similar density $\langle g_S \rangle = 0.6$. In this case, the role of geometrical constraints imposed by excluded volume effect in the real and simulated system should be comparable.

As concerns the simulated decay curve 2 in Figure 4, the association number and the length of insoluble blocks are realistic, the average segment density is comparable with that of the system studied experimentally, numbers of acceptors in the simulated and the real micellar cores are similar, and the ratios of the Förster radius-to-core radius are very similar in both systems (the experimental Förster radius for the carbazole-to-anthracene energy transfer is ca. 2.9 nm).[9a] Curves 1 and 1′ correspond to the calculated and the experimental decays for the polymer-attached carbazole, respectively.

The curves do not coincide precisely because the fluorescence decay from the covalently attached carbazole is not single exponential. Theoretical curve is not the fit of experimental data, however, it is a single exponential decay for the longest lifetime obtained by multiexponential fitting the experimental curve. The comparison of curves 2 and 2′ is fairly good and shows that the model may be used at the semiquantitative level for predictions of basic trends and the most important features of the fluorescence behavior of micellar systems with tagged core-forming blocks. Together with the aforementioned finding that distribution curves obtained by simulations on small and large systems are comparable (if the dimensionless distance normalized by the radius of the core, R, i.e., (r/R) is used) it allows us to draw the conclusion that fluorescence data on smaller systems, which we can study in acceptable CPU times, yield relevant information on realistic micellar systems.

Simulation of Excitation Energy Migration (EEM) and Time-Resolved Fluorescence Depolarization in Equilibrated Micellar Cores. The time-resolved fluorescence anisotropy, $r(t)$, for vertically polarized excitation pulses is defined by[21]

$$r(t) = [F_v(t) - F_h(t)]/[F_v(t) + 2F_h(t)] \qquad (5)$$

where $F_v(t)$ and $F_h(t)$ are the vertically and horizontally polarized time-resolved fluorescence emissions, respectively. In micellar systems with tagged core-forming blocks, the anisotropy decay is due, in part, to the complex rotational diffusion-like motion of pendant fluorophores in micellar cores and to the excitation energy migration (EEM) among fluorophores which are (at least some of them) located to each other relatively closely. Rotational diffusion of whole micelles occurs at incomparably longer time scale than fluorescence decays of typical fluorophores, and this slow motion is therefore not monitored by the time-resolved fluorescence measurements. In very selective solvents (e.g., block polyelectrolyte micelles in aqueous mediate[9b−e]), the rotational motion of pendant fluorophores embedded in compact and rigid micellar cores is frozen, and its contribution to the fluorescence depolarization is negligible. Processes of time-resolved fluorescence depolarization due to energy migration have been studied by several authors,[22] and it has been shown that the time-resolved fluorescence anisotropy may be expressed by the expression[22g]

$$r(t) = r_0(t = 0)[a\, G^S(t) + b] \qquad (6)$$

where the first term, $r_0(t = 0)$, describes the initial anisotropy at the instant of excitation. The initial anisotropy depends on the mutual orientation of transition dipole moments of absorption and emission and for a given fluorophore and a given wavelength is constant. The second term, $G^S(t)$, reflects the excitation energy migration. $G^S(t)$ describes the ensemble average probability that at time t, the excitation is localized at the fluorophore that was originally excited at time $t = 0$. Constants a and b depend on the system studied. The numerical value of b is usually fairly low as compared with a, and its contribution may be neglected in a system of disorganized frozen fluorophores.[22g,h]

As compared with the excitation energy transfer from a fluorophore to traps, theoretical treatment of the excitation energy migration among chemically identical fluorophores is more difficult. One of the first papers on this subject was the work of Haan and Zwanzig.[22a] Later, a cumulant expansion method, which provides a general solution of EEM among fluorophores in infinite volume, was developed by Huber,[22b] and finally, Fayer *et al.*[22c−e] published solutions of EEM for several finite geometries. Our computer-aided stochastic approach allows for numerical evaluation of the experimentally available fluorescence anisotropy decay. This average decay is calculated on the basis of a fairly large ensemble of solutions of the so-called "master equation" that describes energy migration in individual simulated micellar cores. Computer simulations were performed in three steps:

(i) As soon as one equilibrated micellar core with N chains of the length L is created, $N_F \leq N$ random chain ends are "labeled" by fluorophores. Only one fluorophore is "excited", which corresponds to the usual experimental conditions.

(ii) The master equation that describes excitation energy migration[22a] is solved for a great number of simulated configurations, $K(\boldsymbol{r}_1, \ldots, \boldsymbol{r}_{N_F})$, of N_F fluorophores

$$dP_j(K,t)/dt = -P_j(K,t)/\tau_0 + \sum_i w_{ij}[P_i(K,t) - P_j(K,t)] \qquad (7)$$

$P_j(K,t)$ is the probability that for a given configuration $K(\boldsymbol{r}_1, \ldots, \boldsymbol{r}_{N_F})$, the excitation is localized at the jth fluorophore at time t, w_{ij} is the energy transfer rate between fluorophores i and j ($w_{jj} = 0$), and τ_0 is the fluorescence lifetime of the donor. For the dipole−dipole interaction, the excitation energy transfer rate is expressed by the Förster formula[16] (eq 1). The first term of the rhs of eq 7 describes the depletion rate of the excited state by various radiative and nonradiative processes, and the sum of differences $\sum_i w_{ij}[P_i(K,t) - P_j(K,t)]$ describes the process of excitation energy migration. Equation 7, where $i,j = 1, \ldots, N_F$, was transformed into a set of linear equations (using the Laplace transform of $P_{ij}(K,t)$ functions) and solved numerically.

(iii) The time-dependent probabilities that excitation at time t is located on the initially excited fluorophore, either because the excitation has not been transferred to another fluorophore or because it has been transferred from and returned to the initially excited fluorophore, are averaged in an ensemble of ca. 10^5 "individually excited" micelles, and the experimentally observable average function, $G^S(t)$, is obtained. The time-dependent decays of $G^S(t)$ were evaluated for several systems with fixed numbers of fluorophores in all micelles (FNF), as well as for systems with the Poisson distribution of fluorophores among micelles (PDF). Since creation of one equilibrated micelle is considerably more time-consuming than the numerical solution of the set of equations derived from eq 7, several random fluorophores in one equilibrated micellar core were successively "excited". This modification accelerates the simulation procedure and improves statistics of simulated data. Depolarization functions, $G^S(t)$, for FNF systems with different fixed numbers of either randomly distributed (RD) or the end-attached fluorophores in all micelles (SD) and those for systems with the Poisson distribution of end-attached fluorophores among individual micelles (PDF) were calculated (they are not shown, but they may be provided upon request).

A summarized comparison of depolarization functions $G^S(t)$ for systems with fixed number of fluorophores (FNF, solid lines) and with the Poisson distribution of fluorophores (PDF, dashed lines) is shown in Figure 5

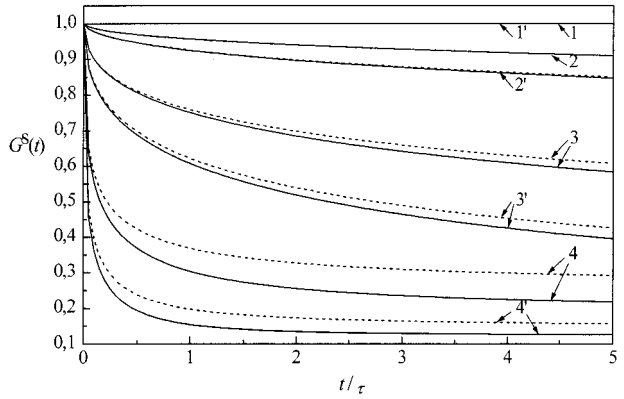

Figure 5. Depolarization function, $G^S(t)$, for the micellar system ($N/L = 15/112$) with the Poisson distribution function (PDF) (dashed line) and a fixed number of fluorophores (FNF) (solid line) for various critical radii ($R_0 = 0.5l$ (1), $2.5l$ (2), $5.0l$ (3), and $10.0l$ (4)). The average and fixed numbers of fluorophores are five (marks without prime) and eight (marks with prime), respectively.

for $N/L = 15/112$, $R = 10l$, and several increasing values of the critical radius, R_0. Couples of curves with numbers without prime correspond to $N_F = 5$ and those with prime to $N_F = 8$. Similar to the NRET equation (eq 4), the EEM equations that describe the time-resolved depolarization of fluorescence are strongly nonlinear in N_F, it is impossible to discuss the effect caused by the Poisson distribution of fluorophores among micelles in a straightforward manner. However, we have shown in the Appendix 2 that the residual value of the depolarization function $G^S(t)$ at long times is always higher in PDF systems than in FNF systems. Simulated data show that the recalculation of spatial distribution of fluorophores from experimental anisotropy decays is a fairly ambiguous problem that requires reliable additional information.

Systems Perturbed by the Presence of Fluorescent Tags. Fluorometric studies on tagged polymer systems may be negatively influenced by a certain perturbation of the system due to introduction of extrinsic fluorophores.[23] Potential danger may be minimized when the fluorophore is chosen to be chemically similar to polymer segments; however this danger still remains. In fluorescence depolarization experiments, potential aggregation of fluorophores might invalidate the analysis based on a model of an unperturbed system.

Fluorescence anisotropy decays that we measured for some micellar systems with end-tagged insoluble blocks[9d,e] differ significantly from the simulated decays. An example is shown in the insert in Figure 6 [Procházka, K; Kiserow, D; Webber, S. E. Unpublished data]. We believe that this type of the anisotropy decay curve may be caused by clustration of fluorophores due to favorable fluorophore-fluorophore interactions. To support this hypothesis, we have calculated the $G^S(t)$ function for a predefined model system of three clusters: two clusters consisting of three fluorophores and one cluster of two fluorophores form an equilateral triangle centered at the center of a micellar lattice; the distance between the core center and the center of each cluster is $4.0l$, and distance between fluorophores in each cluster is $2(^2/_3)^{1/2}l$. Figure 6 shows the $G^S(t)$ functions for several values of R_0. Curve 3 corresponds to the system with a large value of the critical radius. Processes of energy migration among all N_F fluorophores are very fast. The initial drop is extremely steep since energy migration within individual clusters proceeds on

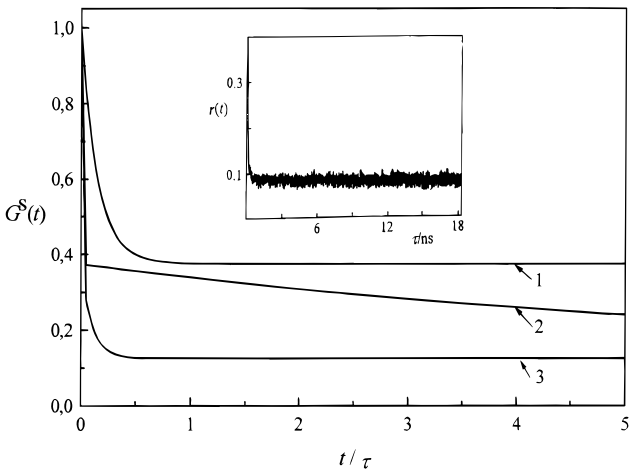

Figure 6. Depolarization function, $G^S(t)$, for system with three clusters of fluorophores. There are eight fluorophores ($R_0 = 2.5l$ (1), $5.0l$ (2), $10.0l$ (3)) in a core. The radius of the spherical core is $10.0l$. Configuration of fluorophores is the following: two clusters consisting of three fluorophores and one cluster of two fluorophores form an equilateral triangle centered at the center of a micellar lattice, with distance between the core center and the center of each cluster being $4.0l$ and distance between fluorophores in each cluster being $2(^2/_3)^{1/2}l$. Insert: experimental time-resolved fluorescence anisotropy, $r(t)$ [Procházka, K.; Kiserow, D.; Webber, S. E. *unpublished experimental data*], for mixed polystyrene-*block*-poly(methacrylic acid) micelles with 10% end-tagged polystyrene blocks in aqueous buffer, pH 9, concentration of copolymer, $c = 5 \times 10^{-3}$ g/mL, excitation at 298 nm, emission at 314 nm, and details of the experimental setup used described in ref 9d,e.

a very short time scale. The residual value of $G^S(t)$ equals 0.125 which is the $(1/N_F)$th part of its original value. In a restricted system containing a limited number of N_F randomly oriented and fixed fluorophores with critical radius comparable with the core radius (curve 3), the energy migration is faster than the depletion of the excited state and the excitation energy at long times after excitation is distributed uniformly among all fluorophores. For low values of the critical radius (significantly lower than the intercluster distance), the energy migration occurs within individual clusters only (curve 1), and the fast initial decay is followed by a high constant anisotropy during quite a long time interval until the complete depletion of the excited state of the fluorophore. In the model system, the residual value of $G^S(t)$ function equals to the expected value $0.375 = [3(^1/_3) + 3(^1/_3) + 2(^1/_2)]/8$. The obtained value $0.375r_0$ is the weighted average from individual clusters (calculated on the basis of expected residual values of $G^S(t)$ function in individual clusters and numbers of fluorophores in them). Curve 2 depicts the case when the value of R_0 allows very fast depolarization within individual clusters and a fairly limited energy transfer between clusters. The initial drop in $G^S(t)$ is very fast due to depolarization within clusters to the value 0.375, and then a slow decrease follows due to the intercluster communication. The most striking feature of the depolarization curve is the sharp transition between the two time regimes.

The comparison of the experimental curve $r(t)$—in the insert (Figure 6)—with the theoretical curves $G^S(t)$ for the model system with the clusters of fluorophores suggest that the high residual anisotropy might be caused by the clustration of fluorophores. Despite the fact that the last system studied was artificially constructed, it gives a good example of what might happen in fluorescence anisotropy measurements on real mi-

cellar systems, and it considerably helps one to understand the experimental depolarization curves.

Conclusions

Simulated data on dense systems of tethered chains enclosed in small volumes allow for evaluation of functions that characterize behavior of such systems in detail. The two-variable function $P_{TF}^{(r)}$ (r_{TF}, φ), which describes distribution of lengths of end-to-end vectors and their orientations, provides a fairly detailed conformational characterization of self-avoiding tethered chains in geometrically constrained systems and shows a correlation between r_{TF} and φ values. Other simulated functions help to understand fluorometric measurements on tagged micellar systems. In this work we have studied systems with (a) random spatial distribution (RD) of solubilized fluorescent tags (either fluorophores of the same type, or donors and traps), (b) simulated (SD) spatial distribution of tags that are attached at the ends of core-forming blocks and with fixed number of tags (SD-FNT) in all micelles, and (c) the Poisson distribution of the end-attached tags among micelles (SD-PDT).

1. Theoretical studies of nonradiative energy transfer based on the simulated distribution of donor-to-trap distances, $n_{FF}(r_{FF})$, in systems that model the tagged micellar cores show that the donor fluorescence decays for individual systems mutually differ. However, all decay curves are very similar to each other, and it is almost impossible to discriminate between them from an experimental point of view.

2. Diffusive processes of excitation energy migration in tagged micellar cores have been also studied by computer simulations. The time-resolved depolarization function, $G^S(t)$, that describes the time-resolved fluorescence anisotropy decay due to energy migration among fluorophores has been calculated. It has been found that fluorescence anisotropy decays for individual systems slightly differ from each other; however, differences are not important.

3. Introduction of fluorophores may perturb the studied system and provoke, e.g., a certain clustration of fluorophores. The simulated anisotropy decay curve for a system containing clusters of fluorophores differs significantly from curves for systems formed by the self-avoiding tethered chains without strong specific interactions between fluorophores. The striking similarity of simulated curves for systems containing clusters with experimental anisotropy decays for some systems studied earlier[9d,e] suggests that the clustration of fluorophores in systems should be taken into account and investigated in more detail.

Acknowledgment. This work was partially supported by Grant No. 203/97/0249 (Grant Agency of the Czech Republic) and by Charles University Grant No. 1197/1997. The authors thank Prof. P. Munk from the University of Texas at Austin, Prof. M. I. Winnik from the University of Toronto, Toronto, Canada, and Prof. W. L. Mattice from the University of Akron, Akron, Ohio, for helpful discussions and suggestions.

Appendix 1

In this part we will show that the time-resolved donor fluorescence decay, $F_D^F(t)$, in a system with a fixed number of traps, μ, in all micelles is always faster than that in the corresponding system with the Poisson distribution of fluorophores among micelles, $F^P{}_D(t)$. For systems with the Poisson distribution of fluorophores among micelles, parameter μ stands for the average number of fluorophores in the system. For simplicity we use in Appendix 1 the symbol N for the actual number of fluorophores in individual micelles and N_{max} for the maximum allowed number of fluorophores *per* micelle.

The decay in both systems may be expressed as follows

$$F_D^F(t) = F_D^0(t)g(t)^\mu \tag{A1}$$

$$F_D^P(t) = F_D^0(t)\sum_{N=0}^{N_{max}} f(N)g(t)^N \tag{A2}$$

where $f(N)$ and $g(t)$ are defined by the following equations

$$f(N) = \frac{e^{-\mu}\frac{\mu^N}{N!}}{\sum_{N=0}^{N_{max}} e^{-\mu}\frac{\mu^N}{N!}} \tag{A3}$$

$$g(t) = \int_0^{2R} \exp[-w(r_{FF})t]n_{FF}(r_{FF})\, dr_{FF} \tag{A4}$$

We have to show that the following generally holds for $t > 0$

$$F^F{}_D(t) < F^P{}_D(t) \tag{A5}$$

After substitution of eqs A1, A2, A3, and A4 into inequality (A5) and after multiplying of both sides of (A5) by the term $\sum_{N=0}^{N_{max}}(\mu^N/N!)$, we get

$$\sum_{N=0}^{N_{max}}\frac{\mu^N}{N!}g(t)^\mu < \sum_{N=0}^{N_{max}}\frac{\mu^N}{N!}g(t)^N \tag{A6}$$

In the systems studied, all members for $N > \mu$ in the sum in the right-hand-side of the inequality (A6) are smaller than the corresponding members in the left-hand-side ($0 < g(t) < 1$). If the relation A6 is fulfilled for the sum from 0 to $N_{max} \to \infty$, then it will be fulfilled also for any finite N_{max}. After simple algebraic rearrangements, we get

$$1 < h(g) = \sum_{N=0}^{\infty}\frac{\mu^N}{N!}g(t)^{(N-\mu)}e^{-\mu} \tag{A7}$$

Function $g(t)$ is defined for times, $t \in (0;\infty)$, and its possible values are in the following region, $0 < g(t) < 1$. For $g(t)\to 0$, $h(g)\to\infty$, and for $g(t)\to 1$, $h(g)\to 1$. To prove that the relation A7 is fulfilled, it is quite sufficient to prove that the function $h(g)$ is decreasing in the interval $g(t) \in (0;1)$. We have therefore to prove that $\partial h/\partial g < 0$. The derivative yields

$$\sum_{N=0}^{\infty}\frac{\mu^N}{N!}e^{-\mu}(N-\mu)g(t)^{(N-\mu-1)} < 0 \tag{A8}$$

This relation may be easily simplified into the final simple form

$$(g(t) - 1) < 0 \tag{A9}$$

which means that the derivative is negative in the

interval $0 < g < 1$. The last inequality defines the interval of $g(t)$ where the function $h(g)$ is continuously decreasing and provides the proof of the relation A7 and consequently of the relation A5.

Appendix 2

In this part we show that the residual anisotropy due to energy migration, i.e., the limiting value of the function $G^S(t)$ for long times, in systems with the fixed number of fluorophores, μ, in all micelles (for $\mu \geq 2$) is generally lower than that in corresponding systems with the Poisson distribution of fluorophores among micelles. In a system with the Poisson distribution, μ stands for the average number of fluorophores and the symbol N will be used for the actual numbers of fluorophores in individual micelles.

In a constrained system (i.e., in one micellar core consisting of N_{max} chains) with a fixed number of μ fluorophores, the limiting residual value of the depolarization function is $G^S(t) = 1/\mu$. In the system with the Poisson distribution, each micelle containing N fluorophores contributes to the ensemble average by the value $1/N$. We want to show that the following relation is fulfilled for $\mu \geq 2$

$$\frac{\sum_{N=1}^{N_{max}} \frac{e^{-\mu}\mu^N}{N!}\frac{1}{N}}{\sum_{N=1}^{N_{max}} \frac{e^{-\mu}\mu^N}{N!}} > \frac{1}{\mu} \qquad \text{(A10)}$$

After simple rearrangements we get

$$\frac{\mu}{2} + \sum_{N=2}^{N_{max}} \frac{\mu^N}{N!}\frac{1}{N(N+1)} > 1 \qquad \text{(A11)}$$

Since the second term in the left-hand-side of relation A11 is positive, the relation is fulfilled for $\mu \geq 2$.

References and Notes

(1) Tuzar, Z.; Kratochvíl, P. In *Surface and Colloid Science*; Matijevic, E., Ed.; Plenum Press: New York, 1993; Vol. 15 and the references cited therein.

(2) (a) Procházka, K.; Kiserow, D.; Webber, S. E. *Acta Polym.* **1995**, *46*, 277. (b) Zhao, C.-L.; Winnik, M. A.; Reiss, G.; Croucher, M. D. *Langmuir* **1990**, *6*, 514. (c) Wilhelm, M.; Zhao, C.-L.; Wang, Y.; Xu, R.; Winnik, M. A. *Macromolecules* **1991**, *24*, 1033. (d) Nakashima, K.; Winnik, M. A.; Dai, K. H.; Kramer, E. J.; Washiyama, J. *Macromolecules* **1992**, *25*, 6866. (e) Hruska, Z.; Piton, M.; Yekta, A.; Duhamel, J.; Winnik, M. A.; Riess, G.; Croucher, M. D. *Macromolecules* **1993**, *26*, 1825.

(3) (a) Kalyanasudaram, K. *Photochemistry in Microheterogeneous Systems*; Academic Press: Orlando, FL, 1987. (b) Turro, N. J.; Grätzel, M.; Braun, A. *Angew. Chem., Int. Ed. Engl.* **1980**, *19*, 675 and references cited therein. (c) Honda, K., Ed. *Photochemical Processes in Organized Molecular Systems*; North Holland Publ.: Amsterdam, 1991.

(4) (a) Leibler, L.; Orland, H.; Wheeler, J. C. *J. Chem. Phys.* **1983**, *79*, 3550. (b) Noolandi, J.; Hong, M. H. *Macromolecules* **1983**, *16*, 1443. (c) Whitmore, D.; Noolandi, J. *Macromolecules* **1985**, *18*, 657. (d) Meier, D. J. *J. Polym. Sci.* **1969**, *C 26*, 81. (e) Helfland, E.; Tagami, Y. *J. Polym. Sci.* **1971**, *B 9*, 741. (f) Helfland, E.; Sapse, A. M. *J. Chem. Phys.* **1975**, *62*, 1327. (g) Nagarajan, R.; Ganesh, K. *J. Chem. Phys.* **1989**, *90*, 5843. (h) ten Brinke, G.; Hadziioannou, G. *Macromolecules* **1987**, *20*, 486. (i) Halperin, A. *Macromolecules* **1987**, *20*, 2943. (j) Halperin, A.; Tirrell, M.; Lodge, T. P. *Adv. Polym. Sci.* **1991**, *100*, 31. (k) Dan, M.; Tirrell, M. *Macromolecules* **1993**, *26*, 4310. (l) Linse, P.; Malmstren, M. *Macromolecules* **1992**, *25*, 5434. (m) Linse, P. *Macromolecules* **1993**, *26*, 4437; **1994**, *27*, 2685; **1994**, *27*, 6404. (n) Hurter, P. N.; Scheutjens, J. M. H. M.; Hatton, T. A. *Macromolecules* **1993**, *26*, 5030, 5592. (o) Gruen, D. *J. Phys. Chem.* **1985**, *89*, 146, 153. (p) Ben-Shaul, A.; Szleifer, I.; Gelbart, W. M. *J. Chem. Phys.* **1985**, *83*, 3597. (q) Szleifer, I.; Ben-Shaul, A.; Gelbart, W. M. *J. Chem. Phys.* **1985**, *83*, 3612; **1986**, *85*, 5345; **1987**, *86*, 7094.

(5) (a) Owenson, B.; Pratt, L. R. *J. Phys. Chem.* **1984**, *88*, 2905, 6048. (b) Rodriques, K.; Mattice, W. L. *Polym. Bull.* **1991**, *25*, 239. (c) Rodriques, K.; Mattice, W. L. *J. Chem. Phys.* **1991**, *94*, 761. (d) Rodriques, K.; Mattice, W. L. *Langmuir* **1992**, *8*, 456. (e) Wang, Y.; Mattice, W. L.; Napper, D. H. *Macromolecules* **1992**, *25*, 4073. (f) Wang, Y.; Mattice, W. L.; Napper, D. H. *Langmuir* **1993**, *9*, 66. (g) Adriani, P.; Wang, Y.; Mattice, W. L. *J. Chem. Phys.* **1994**, *100*, 7718. (h) Nguyen-Misra, M.; Mattice, W. L. *Macromolecules* **1995**, *28*, 1444; **1995**, *28*, 6976. (i) Wijmans, C. M.; Linse, P. *Langmuir* **1995**, *11*, 3748.

(6) Grest, S. G.; Murat, M. In *Monte Carlo and Molecular Dynamics Simulation in Polymer Science*; Binder, K., Ed.; Oxford University Press: New York, 1995 and the references cited therein.

(7) (a) de Gennes, P.-G. *C. R. Acad. Sci. (Paris)* **1985**, *300*, 839. (b) Alexander, S. N. *J. Phys. (Paris)* **1977**, *38*, 983. (c) Milner, S. T.; Witten, T. A.; Cates, M. E. *Macromolecules* **1989**, *22*, 853. (d) Ball, R. C.; Marko, J. F.; Milner, S. T.; Witten, T. A. *Macromolecules* **1991**, *24*, 693. (e) Semenov, A. N. *Sov. Phys. JETP* **1985**, *61*, 733. (f) Birsthein, T. M.; Zhulina, E. B. *Polymer* **1989**, *30*, 170. (g) Zhulina, E. B.; Borisov, O. V.; Pryamitsyn, V. A.; Birshtein, T. M. *Macromolecules* **1991**, *24*, 140.

(8) Zhulina, E. B.; Lyatskaya, Yu. V.; Birshtein, T. M. *Polymer* **1992**, *33*, 332.

(9) (a) Procházka, K.; Bednář, B.; Mukhtar, E.; Svoboda, P.; Trněná, J.; Almgren, M. *J. Phys. Chem.* **1991**, *55*, 4563. (b) Ramireddy, C.; Tuzar, Z.; Procházka, K.; Webber, S. E.; Munk, P. *Macromolecules* **1992**, *25*, 2541. (c) Procházka, K.; Kiserow, D.; Ramireddy, C.; Tuzar, Z.; Munk, P.; Webber, S. E. *Macromolecules* **1992**, *25*, 454. (d) Kiserow, D.; Procházka, K.; Ramireddy, C.; Tuzar, Z.; Munk, P.; Webber, S. E. *Macromolecules* **1992**, *25*, 461. (e) Procházka, K.; Webber, S. E.; Munk, P. *J. Fluoresc.* **1994**, *4*, 353.

(10) (a) Limpouchová, Z.; Procházka, K. *Collect. Czech. Chem. Commun.* **1993**, *58*, 2290; **1994**, *59*, 803. (b) Procházka, K.; Limpouchová, Z. *Collect. Czech. Chem. Commun.* **1994**, *59*, 782; **1994**, *59*, 2166. (c) Procházka, K. *J. Phys. Chem.* **1995**, *99*, 14108.

(11) Rosenbluth, M. N.; Rosenbluth, A. W. *J. Chem. Phys.* **1955**, *23*, 356.

(12) Metropolis, N.; Rosenbluth, M. N.; Rosenbluth, A. W.; Teller, H. *J. Chem. Phys.* **1953**, *21*, 1087.

(13) Siepmann, J. I.; Frenkel, D. *Mol. Phys.* **1992**, *75*, 59.

(14) Allen, M. P.; Tildesley, D. J. *Computer Simulation of Liquids*; Clarendon Press: London, 1987 (reprinted: New York, 1993).

(15) de Gennes, P.-G. *Scaling Concepts in Polymer Physics*; Cornell University Press: Ithaca, NY, 1979.

(16) Förster, Th. *Ann. Phys. (Leipzig)* **1948**, *2*, 55; *Z. Naturforsch., A* **1949**, *4*, 321.

(17) Michl, J.; Bonačić-Koutecký, V. *Electronic Aspects of Organic Photochemistry*; J. Wiley: New York, 1990.

(18) Mendelsohn, A. S.; de la Cruz, M. O.; Torkelson, J. M. *Macromolecules* **1993**, *26*, 6789.

(19) (a) Infelta, P. P.; Grätzel, M.; Thomas, J. K. *J. Phys. Chem.* **1974**, *78*, 190. (b) Maestri, M.; Infelta, P. P.; Grätzel, M. *J. Chem. Phys.* **1978**, *69*, 1522. (c) Infelta, P. P.; Grätzel, M. *J. Chem. Phys.* **1979**, *70*, 179. (d) Dederen, J. C.; Van der Auweraer, M.; De Schryver, F. C. *Chem. Phys. Lett.* **1979**, *68*, 451. (e) Rothenberger, G.; Infelta, P. P.; Grätzel, M. *J. Phys. Chem.* **1979**, *83*, 1871. (f) Rothenberger, G.; Infelta, P. P.; Grätzel, M. *J. Phys. Chem.* **1981**, *85*, 1850. (g) Gehlen, M. H.; De Schryver, F. C. *Chem. Rev.* **1993**, *93*, 199.

(20) Limpouchová, Z.; Viduna, D.; Procházka, K. Mixed Systems of Tethered Chains in Spherical Volumes. A Model for Cores of Mixed Copolymer Micelles. Submitted to *Macromolecules*.

(21) Lakowicz, J. R. *Principles of Fluorescence Spectroscopy*; Plenum: New York, 1983.

(22) (a) Haan, S. W.; Zwanzig, R. *J. Chem. Phys.* **1978**, *68*, 1879. (b) Huber, D. L. *Phys. Rev. B* **1979**, *20*, 2307, 5333. (c) Ediger, M. D.; Fayer, M. D. *J. Chem. Phys.* **1983**, *78*, 2518. (d) Peterson, K. A.; Fayer, M. D. *J. Chem. Phys.* **1986**, *85*, 4702. (e) Keller, L.; Hussey, D. M.; Fayer, M. D. *J. Phys. Chem.* **1996**, *100*, 10257. (f) Gochanour, C. R.; Andersen, H. C.; Fayer, M. D. *J. Chem. Phys.* **1979**, *70*, 4254. (g) Baumann, J.; Fayer, M. D. *J. Chem. Phys.* **1986**, *85*, 4087. (h) Gochanour, C. R.; Fayer, M. D. *J. Phys. Chem.* **1981**, *85*, 1989.

(23) Ghiggino, K. P.; Roberts, A. J.; Phillips, D. *Adv. Polym. Sci.* **1981**, *10*, 69.

MA970002C